Batteries & Supercaps

Review
doi.org/10.1002/batt.202400607

Chemistry Europe
European Chemical Societies Publishing

www.batteries-supercaps.org

Molecular Engineering and Microstructure Modulation of High-Performance Organic Batteries

Mengpei Qi,[a, b, c] Qiqi Sun,*[d] Yonglin Wang,[c] Qi Lai,[c] Li Wang,[c] Zixuan Chen,[c] Yunhai Zhu,*[c] Aiqing Zhang,[a, b] and Yingkui Yang*[c]

Organic electrode materials (OEMs) featuring high abundance, structural designability, and eco-friendliness, are considered promising candidates for rechargeable metal-ion batteries. Nevertheless, the realization of efficient metal-ion batteries based on OEMs is plagued by the poor intrinsic electronic conductivity and low insolubility of OEMs in common organic electrolytes. Herein, we present a systematic discussion of advancements in the design of OEMs from the perspective of molecular engineering and microstructure modulation, aiming at tuning the electrochemical, physical, and chemical properties of OEMs. Additionally, we elucidate the reaction mechanism of regulation strategies and provide new design directions for OEMs. This review offers essential concepts and perspectives on the development of advanced OEMs for rechargeable batteries.

1. Introduction

Environmental deterioration and resource depletion caused by the overconsumption of non-renewable resources promote the exploitation of clean energy like wind and solar. Consequently, it is imperative to exploit ecological energy storage technologies that call for batteries with cost efficiency, long lifespan, and environmental sustainability.[1] Lithium-ion batteries (LIBs) that dominate portable electronic devices and electrical transportation encounter challenges when used in long-duration storage due to resource availability and cost of the commercial inorganic electrode material. Additionally, the repeated insertion/extraction of guest ions into the rigid crystal structure of inorganic materials contributes to their disintegration and dissolution, resulting in degraded electrochemical performance of low capacity and poor cycle stability.[2] Such performance deterioration is aggravated by large or multivalent ions (e.g. Na^+, K^+, Zn^{2+}, Ca^{2+}, Mg^{2+}, and Al^{3+} ions).[3–8] Therefore, it is vital to develop feasible electrode materials to accommodate various charge carriers for next-generation metal-ion batteries (MIBs).

Recently, organic electrode materials (OEMs) have emerged as the most promising electrode materials due to their superiority in environmental friendliness, low cost, and abundance of sources.[9] Unlike inorganic electrode materials that rely on the reversible intercalation and deintercalation of charge carriers alongside the valence changes of transition metals, the reversible electrochemical redox process in organic electrode materials (OEMs) involves alterations in the covalent states of electroactive organic groups. This process is accompanied by the coordination of charge carriers with active functional groups. Such mechanisms help to mitigate strong interactions with the surrounding environment and minimize the large volume changes ccause by the high charge density of multivalent cations. The flexible structure, weak intermolecular interactions, and special energy storage mechanism of OEMs make it feasible in various metal-ion batteries, including alkali metal ions and multivalent metal ion batteries.[10] Depending on the redox mechanism, the OEMs can be classified into three different groups: n-type, p-type, and bipolar-type.[11–13] N-type OEMs feature electron-deficient groups, which accept electrons upon discharging. Consequently, n-type OEMs undergo a reversal transformation between the eigenstate and reduction state.[11] In contrast, p-type OEMs with electron-rich groups donate electrons accompanied by inserting anions during charging, transforming from eigenstate to oxidation state.[12] Bipolar-type OEMs can experience the oxidation process from eigenstate to oxidation state or the reduction process from eigenstate to reduction state, varying with the working conditions.[13]

Over the past several decades, recent efforts have focused on the development of OEMs in various MIBs. Despite significant progress made, the practical implementation of OEMs in MIBs is constrained by several factors: (1) low percentage of redox-active centers; (2) high solubility in electrolytes; (3) low electronic conductivity.[14] Therefore, numerous initiatives are currently being implemented to effectively address the aforementioned barriers of OEMs in MIBs. Unlike previous reviews of organic electrode materials (OEMs), which primarily focus on recent advancements in novel electroactive organic molecules and energy storage mechanisms, this review emphasizes the interrelationship among molecular composi-

[a] M. Qi, A. Zhang
Key Laboratory of Catalysis and Energy Materials Chemistry of Ministry of Education & Hubei,Wuhan 430074, China

[b] M. Qi, A. Zhang
Key Laboratory of Catalysis and Materials Science, South-Central Minzu University, Wuhan 430074, China

[c] M. Qi, Y. Wang, Q. Lai, L. Wang, Z. Chen, Y. Zhu, Y. Yang
State Key Laboratory of New Textile Materials and Advanced Processing Technologies, Wuhan Textile University, Wuhan 430200, China
E-mail: yhzhu@wtu.edu.cn
ykyang@wtu.edu.cn

[d] Q. Sun
Key Laboratory of Superlight Materials and Surface Technology, Ministry of Education, College of Material Sciences and Chemical Engineering, Harbin Engineering University, Harbin 150001, China
E-mail: sunqiqi@hrbeu.edu.cn

tion, microstructural design, and electrochemical properties. We begin by systematically surveying optimization strategies for OEMs, addressing both molecular engineering (based on molecular composition) and microstructural modulation (based on molecular microstructure). Furthermore, we provide a detailed understanding of the molecular engineering of OEMs from the perspective of electron effects (inductive effects and conjugation effects), and try to present a comprehensive review to summarize the latest advanced OEMs with microstructure modulation in terms of 0D, 1D, 2D, and 3D. Ultimately, the paper addresses the obstacles and future outlooks for the advancement of high-performance OEMs.

2. Classifications of Organic Electrode Materials

OEMs consist of naturally plentiful elements, including carbon, hydrogen, oxygen, nitrogen, and sulfur, and can be synthesized artificially or sourced from biomass materials. At the same time, the molecular structure can be flexibly designed according to the requirements of high electrochemical performance of the materials, and the special energy storage mechanism based on the coordination reaction also provides the possibility for the storage of metal ions, including Li^+, Na^+, K^+, Zn^{2+}. Therefore, the development of various organic electrode materials has thus been undertaken for their application in MIBs. Classified by molecular composition, the OEMs encompass a variety of categories, including but not limited to conductive polymers,[15] carbonyl compounds,[16] organic radicals,[17] imine compounds,[18] organosulfur compounds,[19] azo compounds, cyano-derived and other molecules featuring multiple carbon bonds.

Conductive polymers are extensively utilized in the areas of organic electronics, sensors, electrochromic devices, and energy storage technologies. The redox mechanism of the conductive polymers is shown in Figure 1a, with charge transport delocalized along the backbone. Bipolar-type conductive polymers are featured with high electronic conductivity, which would be beneficial for electron transfer. Various types of conductive polymers have been investigated in advanced batteries, mainly including polyaniline (PANI), polypyrrole (PPy), polythiophene (PTh), and poly (3,4-ethylenedioxythiophene) (PEDOT).[20–23] Despite significant progress gained, their practical implements are restricted by the limited specific capacity due to low available doping levels. In addition, conductive polymers have a sloping charge-discharge plateau due to the charged centers are not separated electronically. To this end, extensive studies have been focused on optimizing the doping ions to improve practical capacity and designing reliable molecular structures to ensure structural stability. PANI often displays a capacity of only half of the theoretical capacity due to the irreversible oxidation of PANI. Ju-Won Jeon et al. developed PANI/poly (2-acrylamido-

Ms. **Mengpei Qi** is currently pursuing a Ph.D. at South-Central Minzu University, where she joined the School of Chemistry and Materials Science in 2022. Her research is primarily focused on the energy storage applications of organic electrode materials.

Dr. **Qiqi Sun** received her Ph.D. from Northeast Normal University in 2024 and is currently a Lecturer at Harbin Engineering University. Her research mainly focuses on novel organic electrode materials, including those for lithium-ion and zinc-ion batteries.

Dr. **Yunhai Zhu** received his Ph.D. degree in Materials Science from Jilin University in 2019. After that, he worked as a research fellow at Jilin University and Changchun Institute of Applied Chemistry, Chinese Academy of Sciences. At the Sep. 2022, he joined the State Key Laboratory of New Textile Materials and Advanced Processing Technologies at Wuhan Textile University as a Professor. His current interests mainly focus on functional materials for electrochemical energy storage.

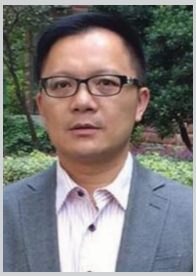

Dr. **Yingkui Yang** is a Professor at the State Key Laboratory of New Textile Materials and Advanced Processing Technologies, Wuhan Textile University, China. He acts as a Fellow of the Royal Society of Chemistry in 2021, and an Associate Editor of Energy & Environmental Materials. He received his PhD degree in Polymer Chemistry and Physics from Huazhong University of Science and Technology in 2007. His current research focuses on crafting polymer-/textile-based advanced materials for electrochemical energy storage.

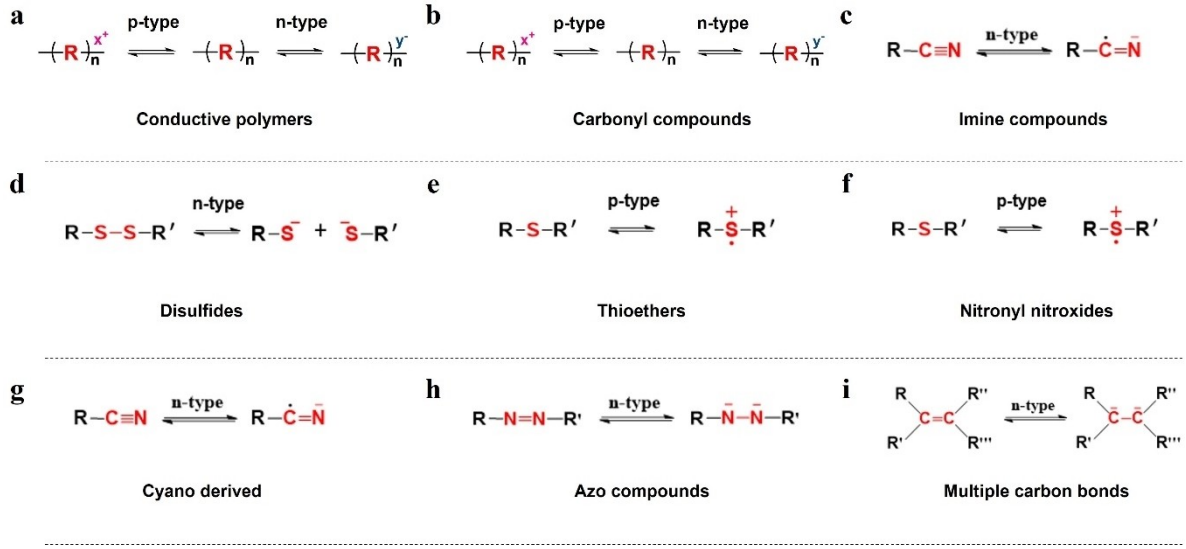

Figure 1. The redox mechanisms of different types of organic electrode materials
a) Conductive compounds. b) Carbonyl compounds. c) Imine compounds. d) Disulfides. e) Thioethers. f) Nitronyl nitroxides. g) Cyano derived. h) Azo compounds. i) Multiple carbon bonds.

2-methyl-1-propanesulfonic acid) (PANI: PAAMPSA)[24] through a complementary ion pairing method. The interaction between the negatively charged anion of the polyacid and the positively charged cation of PANI maintains the completely oxidized state of PANI. Consequently, the PANI/polyacid electrode exhibited a pretty good reversible capacity of 243 $mAh\,g^{-1}$ and a stable lifetime of 800 cycles in LIBs.The enhancement of conductive polymers can be achieved through the optimization of synthesis methods, the optimization of electrolytes, hybridization with inorganic materials, and copolymerizing with other organic monomers.

The high theoretical specific capacity, elevated electrochemical activity, and rapid reaction kinetics of carbonyl compounds render them highly promising as OEMs. Common carbonyl compounds generally include carboxylates, anhydrides, imides, quinones, and ketones. Importantly, the carbonyl (C═O) moiety stands out as the most common n-type organic functional group. It undergoes a reversible single electron transfer reaction to generate a radical intermediate compound and combine with the cations in the electrolyte by the coordination reactions. In other words, the mechanism of redox reactions involving carbonyl compounds occurs via the reversible conversion of carbonyl groups into enols (Figure 1b).[25] During the electrochemical process, only the break and reconstruction of the C═O bonds occur, while the overall molecular structure remains unchanged, resulting in redox kinetics. Recently, a considerable amount of carbonyl compounds has been employed as the electrodes of MIBs. However, the high dissolution and poor electronic conductivity of carbonyl compounds also limit the realization of high performance in MIBs. Song et al. reported poly (benzoquinonyl sulfide) (PBQS) carbonyl polymer as a cathode for rechargeable LIBs. Due to its rational molecular design and high insolubility after polymerization, PBQS exhibits an impressive reversible capacity of 260 $mAh\,g^{-1}$ and displays a great cycling capability of 1000 cycles. As for sodium ion storage, the PBQS exhibited a specific capacity of 268 $mAh\,g^{-1}$ at 50 $mA\,g^{-1}$, similar to the capacity in Li-PBQS batteries. Benefiting from the high average plateaus of 2.08 V, Na-PBQS batteries can deliver an impressive energy density of 557 $Wh\,kg^{-1}$, surpassing the performance of most inorganic cathodes employed in Na-ion batteries.[26] PBQS also provides a high reversible capacity of 203 $mAh\,g^{-1}$ in aqueous zinc-ion batteries.[27] Polyimides have been also investigated in Mg-ion batteries. By conducting a quantitative examination of a quinone polymer (14PAQ) and a polyimide (P(NDI2OD–T2)) throughout the discharge/charge process, Dong and associates proposed that the electrochemical redox mechanism of these polymers in magnesium-ion batteries is chiefly influenced by the combination with $MgCl^+$ instead of Mg^{2+}, especially when assessed in electrolytes containing $Mg_xCl_y{}^+$.[28] All in all, carbonyl electrode materials are stably utilized across various types of ion batteries as electrode components due to their outstanding redox characteristics.

Imine compounds generally refer to a class of organic compounds that contain C═N groups. As shown in Figure 1c, the redox mechanism of imines suggests that the C═N can combine with the cations of electrolytes during the discharge processes. The energy storage mechanism of n-type imine compounds is similar to that of carbonyl compounds with excellent redox activity, significant theoretical specific capacity, and rapid reaction kinetics, but also faces the problems of lower average discharge voltage and poor cycling stability. A novel organic material 5,6,11,12-tetraazanaphthacene (TANC) was first developed by using a heteroatomic substitution strategy.[29] The rational molecular structure effectively lowered the LUMO energy level, resulting in a substantial discharge voltage of 1.15 V in Zn-ion batteries (ZIBs). The large π-conjugated plane with strong π–π interactions not only enhances structural

stability but also boosts charge transfer kinetics. Therefore, the TANC delivers a remarkable reversible capacity of 213 mAh g^{-1} at 0.5 C, an exceptional long-term cycle stability of 47,500 cycles, and an impressive rate capability of 121 mAh g^{-1}, even when operating at 20 C.

Organosulfur compounds are widely utilized as cathodes due to their high voltage and significant specific capacity. Depending on the quantity of sulfur (S) atoms, organosulfur compounds can be classified into three categories: disulfides, polysulfides, and thioethers. Among these, disulfides and polysulfides are classified as n-type organic materials, which undergo redox reactions by reversibly breaking and forming S–S bonds, along with the insertion and removal of cations in electrolytes. Carbonyl and organosulfur compounds that are closely associated are linked together through a click reaction to create 2, 2-((disulfanediylbis(4, 1-phenylene)) bis(azanediyl)) bis(naphthalene-1,4-dione) (MNQ).[30] Benefiting from the multi-functional group composition, enhanced intermolecular interactions, and fast reaction kinetics, the MNQ offers an impressive discharge capacity of 281.2 mA h g^{-1} at the first cycle at 0.5 C, along with reliable cycling performance exceeding 1000 cycles at 1 C. In addition, the more widely studied thioethers are categorized as a p-type material with high voltage. In terms of the redox mechanism in Figure 1d, thioethers first lose electrons without the breakage of bonds, simultaneously interacting with anions that exist in the electrolytes. The first reported thioethers poly [1,4-di(1,3-dithiolan-2-yl) benzene] (PDDTB) is synthesized through a simple oxidative-coupling polymerization method.[31] Research indicates that the S atom within the C–S–C bond is capable of accepting electrons or bearing positive charges in the absence of disulfide bridges, exhibiting greater stability (Figure 1e). The PDDTB delivers an excellent reversible capacity of 378 mAh g^{-1} in rechargeable LIBs. Novel organosulfur compounds are constructed by doping, introduction of heterocycles, or complexation to enhance their structural stability and thus modulate their electrochemical behavior. In conclusion, it is convincing that more efforts dedicated to organsulfides as cathode materials will hold great concern in achieving high-performance metal-ion batteries.[25]

Organic radicals are typical p-type electrode materials. As depicted in Figure 1f, take nitronyl nitroxides as an example, in the redox reaction of organic radicals, only local electron cloud rearrangement occurs, without involving bond breaking and formation, thus possessing rapid kinetics and low voltage polarization. However, organic radicals often exhibit low specific capacity due to high molecular weight, insufficient redox sites, and limited conductivity. In addition, high solubility and severe self-discharge also hinder the further application of organic radicals in MIBs. Therefore, the development of high-performance organic radicals should be mainly guided by efficient structural design and optimization methods. The majority of organic radicals are designed to form the branched chain within the polymers, thereby preventing dissolution and further reinforcing the stability of the radicals. Recently, Xu et al. utilized polypyrrole (PPy) as the primary backbone to create the (2,2,6,6-tetramethylpiperidin-1-yl)oxyl (TEMPO)-containing PPy derivates, creating conductive radical polymers with highly structure stable.[32] This research focused on creating two novel PPy derivatives that contain TEMPO, which have differences in the length of side chains connected to the TEMPO groups. These compounds are designated as 4-(3-(Pyrrol-1-yl) butyryloxy)-2,2,6,6-tetramethylpiperidin-1-yloxy (PPy–B-TEMPO) and 4-(3-(Pyrrol-1-yl) hexanoyloxy)-2,2,6,6-tetramethylpiperidin-1-yloxy (PPy–C-TEMPO). Notably, the increased capacities observed in both electrode materials can be ascribed to their meticulously designed molecular structures. In these structures, the PPy conductive backbone not only improves electron migration but also stabilizes the fully reduced TEMPO through enhanced electron delocalization. Additionally, when compared with PPy–B-TEMPO, the longer and flexible linking side chain of PPy–C-TEMPO allowed for rapid transport of charge carriers within the bulk of the aggregated polymer. Beyond that, organic radical compounds can also enhance ion transport through cross-linking reactions and the introduction of redox mediators in MIBs. In addition to the conventional OEMs mentioned above, some n-type organic compounds based on C≡N, N=N, C=C, and C≡C have been proven to be feasible in MIBs (Figures 1g–i).

3. Molecular Engineering of OEMs

3.1. Adjustment of Redox Centers to Modulate Specific Capacity

The theoretical capacity (Q) of OEMs can be calculated using following equation:

$$Q = \frac{nF}{3.6M_w}$$

where n denotes the count of electrons transferred during the redox reaction, F symbolizes the Faraday constant, and M_w refers to molecular weight. The high theoretical capacity of OEMs can be attained by decreasing molecular weight and promoting reactions that engage multiple electrons. For instance, Anthraquinone (AQ) can participate in a reaction involving two electrons, thereby approaching an accurate theoretical capacity of 257 mAh g^{-1}. By removing the inactive components of AQ gradually, the obtained naphthoquinone (NQ) and benzoquinone (BQ) with theoretical capacities of 339 and 496 mAh g^{-1}, respectively (Figure 2a). However, the practical capacity of AQ approaches that of NQ due to the symmetric conjugated structures providing increased utilization of active sites (Figure 2b).[33] In other words, the actual capacity is still limited by other factors such as molecular spatial structure and electrical conductivity.

A promising strategy to elevate the theoretical capacity of OEMs involves increasing the quantity of redox-active centers to facilitate multi-electron reactions. BQ is a common carbonyl compound containing two redox-active C=O groups with a remarkable theoretical capacity of 496 mAh g^{-1}. After introducing additional electrochemically active C=O groups, the resultant cyclohexanehexone (C_6O_6) can exhibit a significant

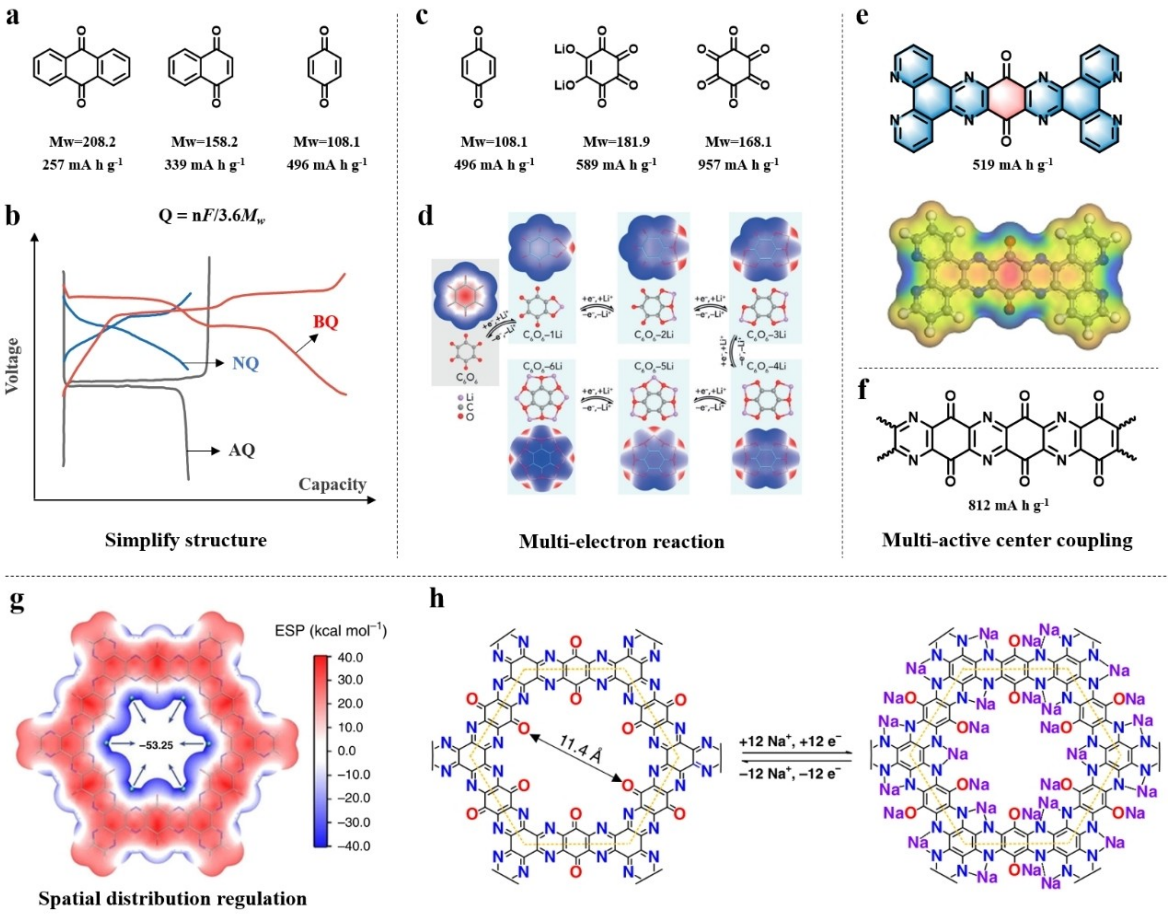

Figure 2. a) Structural formula, molecular weight, and theoretical capacity of AQ, NQ, and BQ. b) Typical charge-discharge curves of AQ, NQ, and BQ.[33] Copyright 2019, The Royal Society of Chemistry. c) Structural formula, molecular weight, and theoretical capacity of BQ, dilithium rhodizonate, and cyclohexanehexone. d) The lithiation process of cyclohexanehexone.[34] Copyright 2022, Springer. e) Structural formula and corresponding molecular electrostatic potential of DQDPD. f) Chemical structure of proposed OEMs with C=N and C=O groups linked alternately.[35] Copyright 2022, Chinese Chemical Society. g-h) Molecular electrostatic potential and electrochemical redox mechanism of TQBQ-COF.[36] Copyright 2020, Nature Publishing Group.

theoretical specific capacity of 957 mAh g^{-1} (Figure 2c). In Figure 2d, the binding of six Li^+ ions with six carbonyl oxygen atoms forms $Li_6C_6O_6$ compounds, leading to a six-electron reaction.[34] Although small molecules typically exhibit high theoretical capacity due to their high concentration of active groups, they often face severe dissolution, leading to irreversible capacity loss. To address this issue and maximize the utilization of ion-storage sites, active groups are typically incorporated into π-conjugated structures or anchored to the polymer skeleton with a liner configuration or 3D framework. However, the balance between structural stability and concentration of active sites should be considered in the structural design of OEMs. Peng et al. recently synthesized a unique organic compound known as dipyrido [3′,2′:5, 6; 2,3:7,8] quinoxalino [2,3-i] dipyrido [3,2-a:2′,3′-c] phenazine-10,21-dione (DQDPD), in which carbonyl and imino groups simultaneously act as active sites to obtain high theoretical capacity. Meanwhile, the prolonged π-conjugated framework ensures high insolubility and facilitates the charge transfer of DQDPD, successfully enhancing the electrochemical behavior in ZIBs (Figure 2e). Notably, DQDPD exhibits a high capacity (509 mAh g^{-1} at 100 mA g^{-1}) along with a ultra-long cycling over 7500 cycles at 10 A g^{-1}. Additionally, the specific capacity and cycling performance can be enhanced by bridging the quinone-based compound with imine nitrogen to form a polymer with a long chain as illustrated in Figure 2f, the active functional groups carbonyl and imino in the polymer chain are simultaneously involved in the redox reactions, resulting in a substantial theoretical capacity of 812 mAh g^{-1}.[35]

Regrettably, the elongated molecular chains result in increased charge transfer barriers, causing the polymers to typically demonstrate slow kinetics, which in turn reduces the utilization of active sites. Regulating the spatial distribution of active groups to make ion-storage sites accessible is indispensable for designing OEMs with high actual capacity. Covalent organic frameworks (COFs) integrate the benefits of porosity, precise structure, and adaptability, offering a promising basis for creating controllable materials that exhibit exceptional performance. In fact, COFs containing multiple carbonyls contribute to affording abundant exposed active sites, thus significantly enhancing electrochemical performance. For example, Shi et al. described a nitrogen-rich honeycomb covalent

organic framework known as TQBQ-COF with a backbone containing tri-quinoxaline and benzoquinone units (TQBQ), in which the carbonyl and pyrazinyl groups are alternately linked (Figure 2g). Since the TQBQ-COF backbone contains multiple active sites, the TQBQ-COF can reversibly uptake 12 Na^+ ions, affording a remarkable theoretical capacity of 515 $mAh\,g^{-1}$ (Figure 2h). Benefiting from the large channel for insertion ion diffusion, the TQBQ-COF demonstrates an exceptionally high specific capacity of 452.0 $mAh\,g^{-1}$. Taking advantage of the extensive pathways available for the diffusion of insertion ions, the TQBQ-COF demonstrates an exceptionally high specific capacity of 452.0 $mAh\,g^{-1}$, which represents a high active site utilization of 88%.[36]

3.2. Inductive Effect to Tailor Working Potential

The enhancement of output voltage also contributes to attaining high energy density of batteries. In general, p-type electrode materials, including organic radicals and thioethers) have a relatively elevated working potential because of their energy storage mechanism. Conversely, n-type organic materials generally show lower working potential and need to be optimized by some strategies. The potential performance of OEMs can be adjusted through molecular engineering approaches. By lowering the energy level of the lowest unoccupied molecular orbital (LUMO), high electron affinity can be achieved, resulting in a high voltage. Therefore, the electrode potentials can be adjusted by incorporating electron-withdrawing functional groups as well as electron-donating groups to fine-tune the chemical environment of active sites.

To achieve a more comprehensive insight into the impact of functional groups on the working potential of OEMs, the potential changes of 1,4-benzoquinone (BQ) and naphthoquinone (NQ) upon the addition of common substituents are summarized. As illustrated in Figure 3a, the addition of electron-donating groups typically results in a lower discharge potential. The degree of voltage decrease is directly related to the strength of the electron-donating ability. Conversely, the incorporation of electron-withdrawing groups leads to a reduction in the LUMO energy level and an increase in electron affinity, which consequently achieves a higher working potential.[37] Li et al. developed two anthraquinone analogs with fused heteroaromatic structures, benzo[1,2-b:4,5-b'] dithiophene-4,8-dione (BDTD) and benzofuro[5,6-b] furan-4,8-dione (BFFD) (Figure 3b). The incorporation of electron-withdrawing atoms O and S atoms has greatly improved the working potential and energy densities of BDTD and BFFD in aqueous zinc batteries. Consequently, the BDTD cathode displays impressive performance of excellent rate property of up to 30 $A\,g^{-1}$, and extended cycle stability for over 12,000 cycles.[38] Similarly, Liu et al. also confirmed that substituents exhibiting various electronic inductive effects can significantly modify the LUMO levels and the energy state of electrons involved in the reduction course, which consequently results in a variation in the reduction potential (Figure 3c).[39] Therefore, the Br-NB with electron-withdrawing bromine (–Br) group displayed higher output voltage when compared with the 4-NT with an electron-donating methyl ($-CH_3$) group. Furthermore, the number of substituent groups also influences the working potential. For example, a higher redox potential of 1,4-benzoquinone derivatives can be obtained by increasing the number of halogen substituents. Significantly, the trend of Na storage redox potential is $C_6F_4O_2 > C_6Cl_4O_2 > C_6Br_4O_2 > C_6H_4O_2$. (Figures 3d, e).[40]

As mentioned above, the introduction of electron-donating groups typically results in a reduction of discharge voltages in OEMs by elevating the LUMO energy. However, the electron-donating groups can also raise the voltage, once the specific gust ion interacts with the groups. Recently, Lee et al. developed how different substituents influence the discharge voltages of OEMs by synthesizing new derivatives of disodium dimethoxy terephthalate (Na2TP) (Figure 3f).[41] They found that disodium terephthalate (Na_2MeO_2TP) exhibited higher discharge voltage than disodium dimethyl terephthalate (Na_2DMTP) in both LIBs and sodium-ion batteries (SIBs), as well as higher than the unsubstituted Na_2TP in LIBs, although the introduced $-OCH_3$ is an electron-donating group. The unforeseen increase in the discharge voltage of Na_2MeO_2TP was determined to arise from the close interaction between the charge-carrying cations and the host molecules. Stable bonds may be formed by the cations with the electronegative oxygen atoms found in the methoxy substituents close to the redox center, leading to the creation of stable six-membered ring structures, which consequently causes a notable increase in the discharge voltage.

3.3. Conjugation Effect to Tune Rate Capability and Cycling Stability

The phenomenon of conjugation effects pertains to the spreading of electrons throughout the entire conjugated framework. In this process, π electrons can delocalize between multiple atoms, thereby reducing the energy of the entire system and enhancing the intermolecular interactions, which can improve both the cyclability and rate performance of OEMs. For example, as one moves from BQ to AQ and then to pentacenetetrone (PT) (Figure 4a), the expansion of π-conjugated structures leads to a gradual reduction in solubility within typical organic electrolytes and an acceleration of π-electron transfer. The conjugation effect mentioned above is also applicable to polymer materials. Recently, Tang et al. have synthesized the corresponding polymers based on BQ, AQ, and PT units under identical conditions, resulting in poly (benzoquinonyl sulfide) (PBQS), poly (anthraquinone sulfide) (PAQS) and poly (pentacenetetrone sulfide) (PPTS), respectively.[42] The expansion of the π-conjugated structure within polymers also contributes to the improved π–π intermolecular interactions and a well-organized layered structure of PPTS, facilitating the rapid diffusion of Na ions. Consequently, PPTS exhibited superior specific capacity, ultra-long cycle stability, and rate performance when compared to PT as well as other similar compounds (PBQS and PAQS). PPTS demonstrated a specific capacity of 290 $mAh\,g^{-1}$ at 100 $mA\,g^{-1}$. Notably, it retained

Review
doi.org/10.1002/batt.202400607
Chemistry Europe
European Chemical Societies Publishing

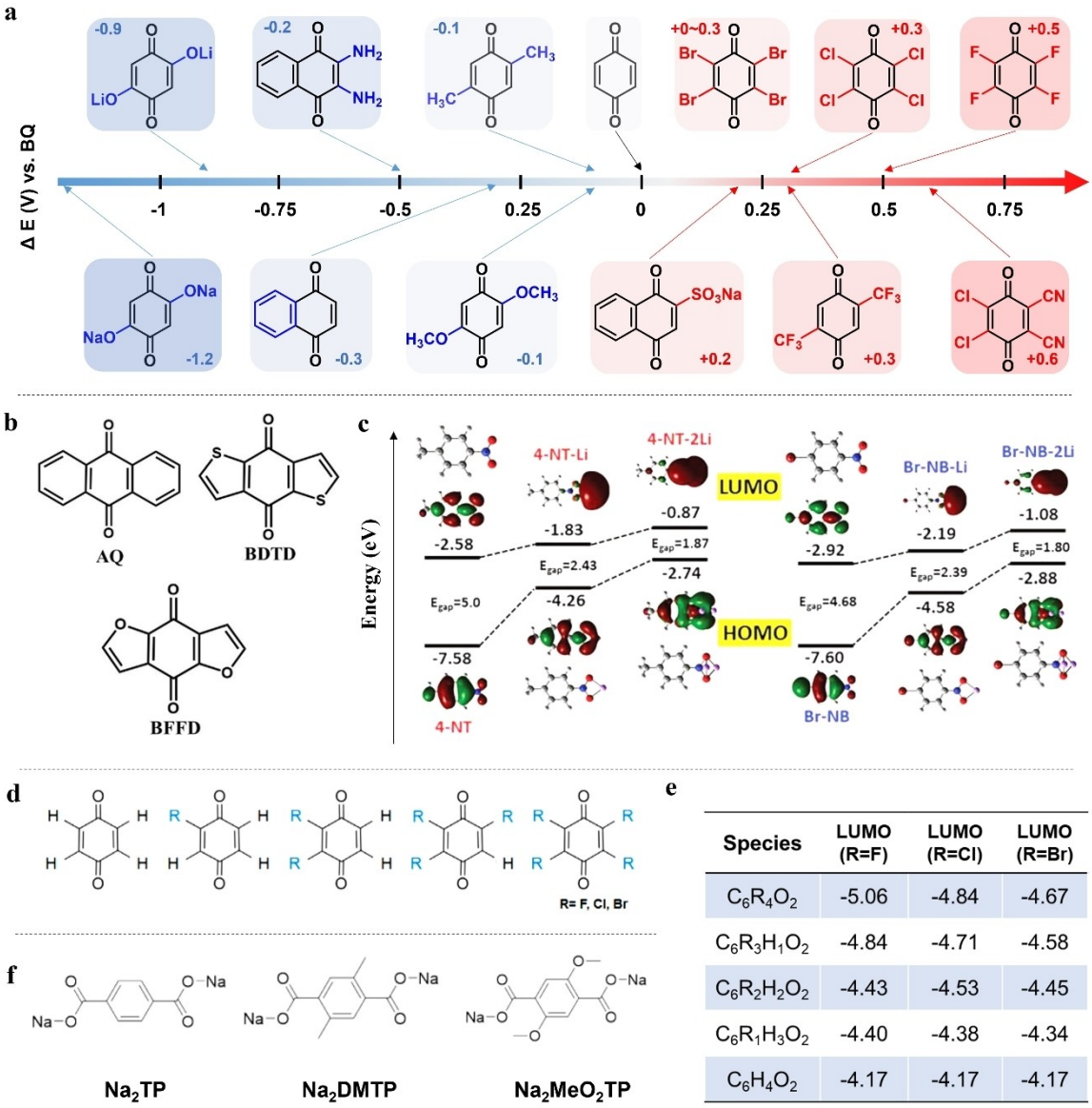

Species	LUMO (R=F)	LUMO (R=Cl)	LUMO (R=Br)
$C_6R_4O_2$	-5.06	-4.84	-4.67
$C_6R_3H_1O_2$	-4.84	-4.71	-4.58
$C_6R_2H_2O_2$	-4.43	-4.53	-4.45
$C_6R_1H_3O_2$	-4.40	-4.38	-4.34
$C_6H_4O_2$	-4.17	-4.17	-4.17

Figure 3. a) Representative electron-withdrawing and electron-donating groups to tune the output voltage of BQ and NQ. b) Molecular structures of the AQ, BDTD, and BFFD.[38] Copyright 2022, Wiley-VCH. c) HOMO/LUMO level evolution for 4-NT and Br-NB during lithiation/de-lithiation process.[39] Copyright 2023, Wiley-VCH. d, e) Chemical structure and LUMO energies of $C_6R_4O_2$ molecules (R=F, Cl, Br).[40] Copyright 2015, American Chemical Society. f) Structural formula of Na_2TP, Na_2DMTP, and Na_2MeO_2TP.[41] Copyright 2019, The Royal Society of Chemistry.

reversible capacities of 100 mAh g^{-1} at 50 A g^{-1} after 10,000 cycles. The excellent performance was derived from the rapid charge transfer and ion diffusion caused by the conjugation effect in polymer electrode material. Notably, Tang et al. also developed the application of PPTS cathode in potassium-ion batteries (PIBs) with excellent rate capability, which could be due to the high diffusion coefficient of K^+ (approximately 10^{-9} cm^2 s^{-1}).[43]

Nonetheless, the extended π-conjugated frameworks typically contain excess inactive components, which ultimately diminishes the theoretical capacity. Therefore, it is also crucial to properly construct abundant active sites while designing extended π-conjugated structures. To this end, Peng et al. proposed to introduce redox actives N-heterocycles to extend the π-conjugation of organic electrodes, which successfully promote charge transport, reduce solubility and provide more active sites at the same time.[35] The novel-developed BQ, known as DQDPD, possesses an elongated N-heterocyclic-conjugated framework. These derivatives were crafted for use as cathodes in ZIBs, offering an impressive theoretical capacity of over 500 mA h g^{-1} (Figure 4b). In addition, the DQDPD electrode has the narrowest bandgap compared with BQ and TAPQ, which once again demonstrates that the extended π-conjugation can also accelerate electron transfer. Introducing dual redox-active centers into molecules with extended conjugated structures enables rapid charge transfer and multi-

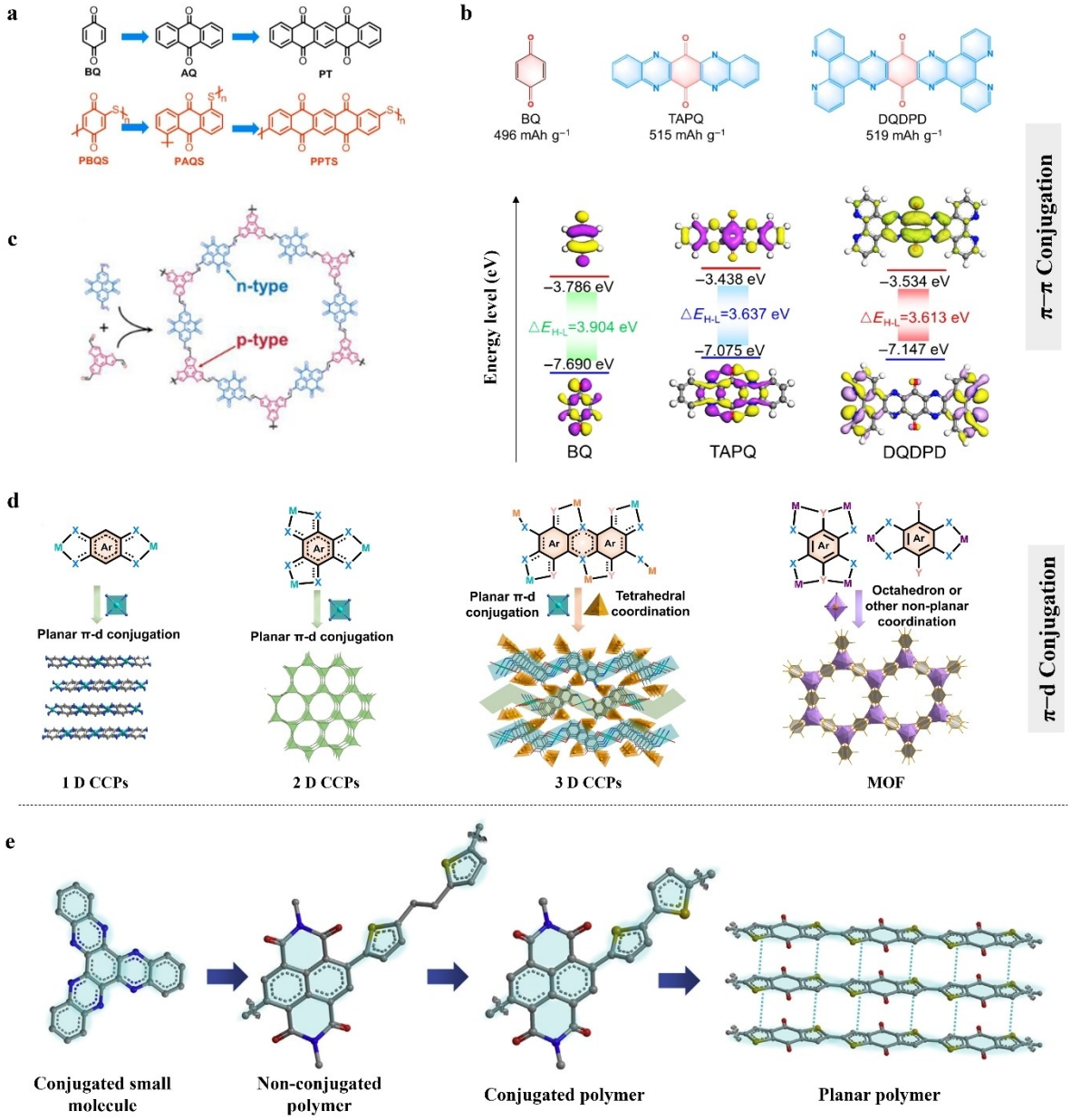

Figure 4. a) Molecular design route of PPTS.[42] Copyright 2018, Elsevier. b) Molecular structures and corresponding HOMO/LUMO energy levels and energy gaps of BQ, TAPQ, and DQDPD.[35] Copyright 2022, Chinese Chemical Society. c)The preparation of BTT-PTO-COF.[44] Copyright 2024, Wiley-VCH. d) Typical design strategies for π-d conjugated configuration.[45] Copyright 2023, American Chemical Society. e) Schematic representation of conjugated small molecule, non-conjugated polymer with conjugated redox-active units, conjugated polymer with conjugated redox-active units, and conjugated polymer with a planar structure and intermolecular interactions.[46] Copyright 2021, Elsevier.

electron redox processes. Recently, Li et al. successfully synthesized a conjugated BTT-PTO-COF electrode with a p-type benzo[1,2-b:3,4-b′:5,6-b″] trithiophene (BTT) and an n-type 4,5,9,10-tetraone (PTO) active center (Figure 4c). Due to the extended conjugated structure within the COF molecular and the presence of dual redox-active groups, the BTT-PTO-COF electrode material demonstrates excellent cycling properties in lithium-ion batteries, achieving 218 mAh g^{-1} at 0.2 A g^{-1} in ether-based electrolytes and 275 mAh g^{-1} at 0.2 A g^{-1} in carbonate-based electrolytes. In addition, the BTT-PTO-COF electrode also exhibits remarkable rate performance (79 mAh g^{-1} at 50 A g^{-1} in ether-based electrolytes and 124 mAh g^{-1} at 10 A g^{-1} in carbonate-based electrolytes).[44]

The incorporation of π-d conjugation serves as a significant approach to enhance the characteristics of electrode materials. Recently, studies have indicated that conjugated coordination polymers (CCPs), which are constructed using organic ligands in conjunction with metal ions, exhibit conductivity or may even demonstrate superconductivity. The interaction between the frontier π orbitals of the conjugated ligands and the d orbitals

of transition metals can improve the electrical conductivity. Furthermore, the π-d conjugation structure can effectively address the dissolution challenges associated with small molecular ligands. Therefore, various π-d CCPs, including 1D, 2D, 3D, and even 3D MOF have been proposed and synthesized (Figure 4d).[45] Fan et al. comprehensively studied the electrochemical reaction of a coordination polymer consisting of Ni^{2+} ions with 1,2,4,5-benzenetetramine (BTA). The π-d conjugation significantly improves the structural stability and conductivity of Ni-BTA. Furthermore, extensive experiments and theoretical analyses revealed that Ni-BTA participates in a three-electron reaction of each unit, during which BTA^{2-} is capable of accepting two electrons to generate BTA^{4-}. This process is associated with the reduction of C=N, while Ni (II) can perform an electron reaction, leading to the formation of highly reactive Ni(I). Highly crystalline H–Ni-BTA demonstrates exceptional electrochemical properties in SIBs, exhibiting a reversible capacity of approximately 500 mAh g^{-1} at 0.1 A g^{-1}, along with outstanding rate performance of 330 mAh g^{-1} at 10 A g^{-1}.

Overall, the conjugation effect in OEMs involves the delocalization of electrons throughout the whole structure through interconnected π orbitals, which offers an extra route for rapid electron transport. Uninterrupted conjugated pathways facilitate efficient electron and ion transport. Therefore, in terms of the conjugated structure design of organic molecules, it is necessary to design a better conjugate system for π-overlapping planes. In a word, a completely planar conjugated system is anticipated to facilitate improved π overlap and yield greater conductivities. (Figure 4e).[46]

4. Microstructure Modulation of Organic Electrode Materials

The molecular engineering strategy aims to customize the electrochemical performance of OEMs by following the relationship between structure and performance. However, the electrochemical performance achieved solely by optimizing the structure of organic molecules themselves is still limited, and the realization of theoretical electrochemical performance often requires the assistance of other strategies. The inherent poor electronic transport of OEMs will not only affect the rate performance but also lead to a decrease in the actual specific capacity due to lower active material utilization of OEMs.[47] To address the aforementioned challenges, microstructure modulation strategies have been employed to improve the electrical characteristics of OEMs and have achieved significant results.

Effective enhancement of electrochemical performance in MIBs can be achieved by regulating the micromorphology of the materials. As shown in Figure 5a, the synthesis of point (zero-dimensional, 0D), line (one-dimensional, 1D), planar (two-dimensional, 2D), and bulk (three-dimensional, 3D) materials on the nanoscale has successfully increased the specific surface

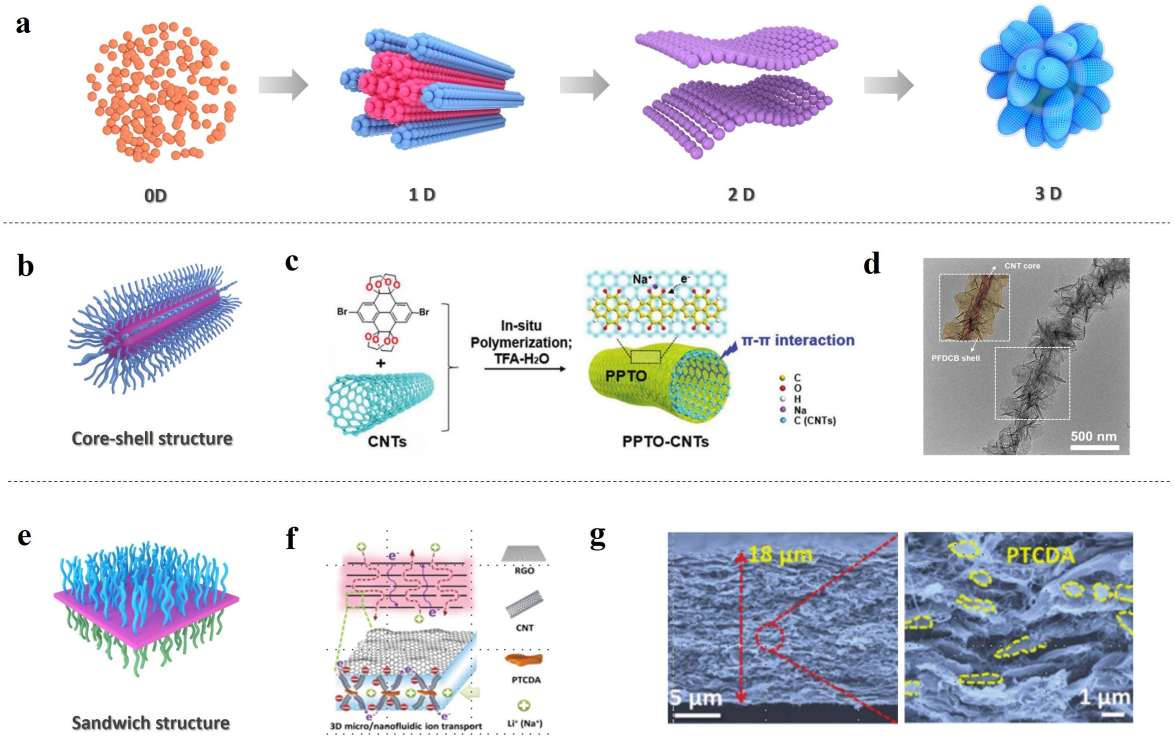

Figure 5. a) Schematic diagram for zero-dimensional material, one-dimensional material, two-dimensional material, and three-dimensional material. b) Schematic diagram for core-shell organic electrode materials. c) Schematic illustration of the in situ polymerization process of PPTO-CNTs composites.[52] Copyright 2020, WILEY-VCH. d) TEM image of CNT@PFDCB.[54] Copyright 2024, WILEY-VCH. e) Schematic diagram for sandwich-like architecture organic electrode materials. f) Schematic illustration for preparation of the bioinspired PTCDA/GO/CNT film with 3D micro/nanofluidic channels. g) Cross-sectional, and middle active layers of PTCDA/RGO/CNT composite film, respectively.[57] Copyright 2018, WILEY-VCH.

area, accelerated ion transport and electron conduction. However, the tendency of nanomaterials to aggregate can affect their cycling stability, and suitable carbon matrices are usually needed to assist in maximizing their electrochemical performance. Nanoscale particles of 0D electrode materials can reduce the ions and electrons transport distances within the materials, thereby enhancing the electrochemical performance. Alexandru Vlad et al. successfully prepared a nanoscale homopolymer composites poly (2,2,6,6-tetra-methylpiperidinyloxy-4-yl methacrylate) with in situ carbon addition ($PTMA_{MP\text{-}iC}$) by a solvent-free and environmentally friendly polymerization method.[48] The surface morphology of the $PTMA_{MP\text{-}iC}$ composites reveals that the melt-polymerized material exhibits a high degree of nanoscale homogeneity. Due to the shorter lithium-ion diffusion paths associated with the 0D nanoparticles, the $PTMA_{MP\text{-}iC}$ electrode materials demonstrate excellent rate performance. Furthermore, over 50% of the capacity is maintained at a cycling rate of 10 C (1 $A g^{-1}$), and the redox plateau persists even at elevated rates surpassing 100 C. Notably, benefiting from its unique nanostructure and effective composite with carbon materials, the $PTMA_{MP\text{-}iC}$ electrode also exhibits outstanding cycling performance of a long lifetime of 1200 cycles maintaining more than 85% capacity retention at 10 C (1 $A g^{-1}$) in LIBs.

1D nanomaterials include nanofibers, nanotubes, and nanorods. 1D organic nanomaterials are commonly assembled into interconnected networks that facilitate rapid ion and electron transport, thereby significantly enhancing cycling stability. This characteristic significantly enhances the electrochemical performance of MIBs. Inspired by the technique of bio-self-assembly, Xing et al. created a high-performance nanostructured N-hydroxynaphthylimine sodium salt (NDI-ONa) cathode in SIBs.[49] The scanning electron microscopy (SEM) images of NDI-ONa reveal remarkably uniform micron-sized one-dimensional fibers. The nanowire structure of NDI-ONa effectively inhibits the aggregation and growth of particles while shortening ions and electrons diffusion paths. As a result, NDI-ONa with a sodium alginate (SA) binder demonstrates remarkable capacity retention of 93% after 20000 cycles at 3 $A g^{-1}$ in SIBs.

2D nanosheet structures exhibit unique surface chemical characteristics, including rapid in-plane electron mobility and a significant abundance of active sites. Wang et al. developed a high redox-active anthraquinone-based COF (DAAQ-ECOF) as the cathode in LIBs which was delaminated into few-layer 2D nanosheets.[50] In contrast to the original COFs, the exfoliated COFs feature shorter Li^+ diffusion pathways, enhanced utilization of redox sites, and improved reaction kinetics of lithium storage. Notably, DAAQ-ECOF demonstrates exceptional cycling stability of 1800 cycles, as well as rapid charge/discharge ability.

Compared with other low-dimensional organic nanomaterials, 3D organic nanomaterials exhibit higher specific surface areas and open electronic transmission channels. Wang et al. constructed a poly(2,3-dithio-1,4-benzoquinone) composite PDB/3D-FC that features a 3D flower-like structure to serve as a cathode in LIBs and SIBs.[51] Apparently, the 3D structure of PDB/3D-FC electrode material evidently enhances the accessibility of active sites, speeds up electron transport, and efficiently mitigates the volume expansion that occurs in the charging/discharging processes. Therefore, the PDB/3D-FC displays an impressive discharge capacity of 203 mAh g^{-1} in LIBs at 1 $A g^{-1}$.

Additionally, unique structural designs of electrode materials have led to significant enhancements in electrochemical properties. Particularly, the construction of a core-shell structure increases the specific surface area and facilitates the efficient transport of electrons and ions. (Figure 5b). To tackle the problems related to cross-linking and inadequate electrical conductivity in polymers, Shi et al. prepared π-conjugated poly (pyrene-4,5,9,10-tetrone) combined with carbon nanotubes (PPTO-CNTs) utilizing an in situ polymerization approach (Figure 5c).[52] Benefiting from the high electronic conductivity and structural stability, the PPTO-CNTs with core-shell structure achieve a high specific capacity of 360.2 mA h g^{-1} at 0.05 $A g^{-1}$, long-term cycling stability of 1300 cycles, and outstanding rate performance of 194.5 mA h g^{-1} at a high current density of 10.0 $A g^{-1}$. Wang et al. have designed 2D crystalline electrode composites of polyarylamide hybrids and carbon nanotubes (2D-PAI@CNT).[53] Significantly, the core-shell structure of the layered heterojunction composite electrode material makes almost all redox active sites accessible, where the 1D inner core CNT transport channel allows for fast electron transport, and the outer shell nanomaterials enable fast lithium-ion storage. Similarly, Wang et al. developed a core-shell nanostructures poly(1,4-dicyanoperfluorobenzene sulfide) (CNT@PFDCB) using an in situ polymerization method (Figure 5d).[54] Favored by the core-shell architecture, the CNT@PFDCB cathode displays an impressive capacity (203.5 mAh g^{-1}), outstanding rate ability (127.6 mAh g^{-1} at 3.0 $A g^{-1}$), and remarkable cycling stability (retaining 81.1% capacity after 3000 cycles at 1.0 $A g^{-1}$ in LIBs.

Graphene is also an inorganic matrix that is highly suitable for the composite with π-conjugated organic materials. Luo et al. constructed a microporous poly(imide-benzoquinone) graphene composites (PIBN–G) cathode in LIBs via in situ polymerization.[55] The PIBN–G cathode material delivers excellent conductivity for electrons as well as effective Li^+ diffusion. Notably, PIBN–G demonstrates remarkable rate performance of 271.0 mAh g^{-1} and 193.1 mA h g^{-1} at 0.1 C and 10 C, respectively. Similarly, Yang et al. developed graphene/carbonyl-enriched polyquinoneimine (PQI@Gr) composites for LIBs.[56] With numerous 3D porous channels and highly exposed active sites, the graphene-sandwiched hierarchical nanoarchitecture is adequate for rapid ion diffusion and enhanced active site utilization, which in turn improves electrochemical performance. Therefore, compared to bare PQI, the PQI@Gr cathode exhibits a remarkable rate capability of 179.4 mA h g^{-1} at 5.0 $A g^{-1}$ and excellent cycling performance of 10,000 cycles at 5.0 $A g^{-1}$. In particular, graphene can be applied to construct sandwich structures, which effectively reduces the self-stacking of graphene nanosheets, improves the utilization of active sites, accelerates ion transport, and is expected to further enhance electrochemical performance (Figure 5e). Benefiting from the non-covalent π-π stacking interactions between graphene oxide (RGO) nanosheets and CNT, the simultaneous utilization of RGO and CNT is more conducive to ion diffusion, thereby promoting the electrochemical performance of the composites in MIBs.

Zhou et al. reported a 3D interconnected micro/nano-fluidic networks 3,4,9,10-perylenetetracarboxylic dianhydride (PTCDA)/reduced graphene oxide (RGO)/carbon nanotube (CNT) (PTCDA/RGO/CNT) composite film in Figure 5f. The cross-sectional SEM images of the PTCDA/RGO/CNT electrode reveal a distinct sandwich-like structure (Figure 5g), in which the RGO and CNT are integrated within the active material PTCDA to construct the active layer. Thanks to the unique flexible sandwich structure, PTCDA/RGO/CNT composites demonstrate significant utilization efficiency of active particles and remarkable cyclic stability. Notably, both LIBs and SIBs exhibited over 99% capacity retention after 500 cycles at 200 mA g^{-1}.[57]

5. Conclusions and Future Perspectives

In summary, organic electrode materials possess the renewability of resources, variety of structures, and design flexibility, which can be used to construct high-performance metal-ion batteries. Nevertheless, the further application of organic materials is still constrained by low intrinsic conductivity, insufficient active sites, and low insolubility. This review offers a summary of the categorization of OEMs and highlights effective modification means to improve the electrochemical performance of different MIBs. The electrochemical performance can be improved by molecular engineering strategies, such as the modulation of active centers, the incorporation of electron-withdrawing groups, and the design of π-conjugated frameworks. In addition, microstructure modulation can also efficiently address the challenges, including the regulation of micromorphology and hybridization with carbon materials. Although significant advancements have been made in the exploitation of OEMs, there is still considerable work to undertake.

Considering the aforementioned issues, we strongly recommend that future investigations of OEMs focus on the following research directions. (1) Precise design of organic molecules: Fine control over the crystallinity, planarity, and other related properties of organic electrode materials (OEMs) is crucial for achieving high electrochemical performance (2) Integration of High-Throughput Screening and Machine Learning: Combining these techniques for the selection and performance prediction of OEMs can accelerate the design process of new organic active materials and simplify the study of redox reaction mechanisms. (3) Investigation of Failure Mechanisms: Focusing on the reasons for the failure of OEMs, along with extending research to electrolyte optimization and separator modification, offers new avenues for the development of advanced battery technologies. (4) Advancement of Characterization Technologies: Emphasizing the development and application of cutting-edge characterization techniques in battery research is imperative. Notably, progress in in-situ characterization technologies has significantly deepened our understanding of internal reaction mechanisms within batteries, providing a solid theoretical foundation for effective optimization strategies. By addressing these critical areas, we can pave the way for the commercialization of OEMs in the near future.

Acknowledgements

This work was financially supported by the National Natural Science Foundation of China (52173091, 51973235, and 52301285), Program for Leading Talents of National Ethnic Affairs Commission of China (MZR21001), and Hubei Provincial Natural Science Foundation of China (2021CFA022).

Conflict of Interests

The authors declare no conflict of interest.

Keywords: Organic electrode materials · Molecular engineering · Microstructure modulation · Metal-ion batteries

[1] a) M. Freire, N. V. Kosova, C. Jordy, D. Chateigner, O. I. Lebedev, A. Maignan, V. Pralong, *Nat. Mater.* **2016**, *15*, 173–177; b) N. Nitta, F. Wu, J. T. Lee, G. Yushin, *Mater. Today* **2015**, *18*, 252–264; c) J. Xie, Y.-C. Lu, *Nat. Commun.* **2020**, *11*, 16259.
[2] a) H. Huang, W. Feng, Y. Chen, J. Shi, *Nano Today* **2020**, *35*, 100972; b) Z. Ma, J. Yu, S. Dai, *Adv. Mater.* **2009**, *22*, 261–285; c) M.-S. Park, J. Kim, K. J. Kim, J.-W. Lee, J. H. Kim, Y. Yamauchi, *Phys. Chem. Chem. Phys.* **2015**, *17*, 30963–30977.
[3] a) C. Delmas, *Adv. Energy Mater.* **2018**, *8*, 1703137; b) M. D. Slater, D. Kim, E. Lee, C. S. Johnson, *Adv. Funct. Mater.* **2012**, *23*, 947–958; c) N. Yabuuchi, K. Kubota, M. Dahbi, S. Komaba, *Chem. Rev.* **2014**, *114*, 11636–11682.
[4] a) X. Ma, H. Fu, J. Shen, D. Zhang, J. Zhou, C. Tong, A. M. Rao, J. Zhou, L. Fan, B. Lu, *Angew. Chem. Int. Ed.* **2023**, *62*, e202312973; b) R. Rajagopalan, Y. Tang, X. Ji, C. Jia, H. Wang, *Adv. Funct. Mater.* **2020**, *30*, 1909486; c) K. Sada, J. Darga, A. Manthiram, *Adv. Energy Mater.* **2023**, *13*, 2302321; d) L. Wang, S. Zhang, N. Li, J. Chen, Y. Chen, Z. Zhang, L. Tan, X. Niu, Y. Yang, J. Zhang, H. Li, X. Ji, Y. Zhu, *Adv. Funct. Mater.* **2024**, 2408965, Doi: 10.1002/adfm.202408965.
[5] a) X. Deng, L. Li, G. Zhang, X. Zhao, J. Hao, C. Han, B. Li, *Energy Storage Mater.* **2022**, *53*, 467–481; b) J. Park, Z. L. Xu, G. Yoon, S. K. Park, J. Wang, H. Hyun, H. Park, J. Lim, Y. J. Ko, Y. S. Yun, K. Kang, *Adv. Mater.* **2019**, *32*, 1904411; c) M. Wang, C. Jiang, S. Zhang, X. Song, Y. Tang, H.-M. Cheng, *Nat. Chem.* **2018**, *10*, 667–672.
[6] a) A. L. Lipson, B. Pan, S. H. Lapidus, C. Liao, J. T. Vaughey, B. J. Ingram, *Chem. Mater.* **2015**, *27*, 8442–8447; b) X. Yu, A. Manthiram, *Chem* **2018**, *4*, 1200–1202; c) Y. Jie, Y. Tan, L. Li, Y. Han, S. Xu, Z. Zhao, R. Cao, X. Ren, F. Huang, Z. Lei, G. Tao, G. Zhang, S. Jiao, *Angew. Chem. Int. Ed.* **2020**, *59*, 12689–12693.
[7] a) R. Deivanayagam, B. J. Ingram, R. Shahbazian-Yassar, *Energy Storage Mater.* **2019**, *21*, 136–153; b) B. T. McAllister, L. T. Kyne, T. B. Schon, D. S. Seferos, *Joule* **2019**, *3*, 620–624; c) R. Mohtadi, O. Tutusaus, T. S. Arthur, Z. Zhao-Karger, M. Fichtner, *Joule* **2021**, *5*, 581–617.
[8] a) S. K. Das, S. Mahapatra, H. Lahan, *J. Mater. Chem. A* **2017**, *5*, 6347–6367; b) F. Wu, H. Yang, Y. Bai, C. Wu, *Adv. Mater.* **2019**, *31*, 1806510; c) C. Yan, C. L. Liu Wang, W. Cui, L. Zhang, K. N. Dinh, H. Tan, C. Wu, T. Wu, Y. Ren, J. Chen, Z. Liu, M. Srinivasan, X. Rui, Q. Yan, G. Yu, *J. Am. Chem. Soc.* **2020**, *142*, 15295–15304.
[9] a) Y. Xu, M. Zhou, Y. Lei, *Mater. Today* **2018**, *21*, 60–78; b) Y. Lu, J. Chen, *Nat. Chem. Rev.* **2020**, *4*, 127–142.
[10] T. Sun, Z. J. Li, H. G. Wang, D. Bao, F. L. Meng, X. B. Zhang, *Angew. Chem. Int. Ed.* **2016**, *55*, 10662–10666.
[11] a) J. E. Anthony, A. Facchetti, M. Heeney, S. R. Marder, X. Zhan, *Adv. Mater.* **2010**, *22*, 3876–3892; b) J. Liu, B. van der Zee, R. Alessandri, S. Sami, J. Dong, M. I. Nugraha, A. J. Barker, S. Rousseva, L. Qiu, X. Qiu, N. Klasen, R. C. Chiechi, D. Baran, M. Caironi, T. D. Anthopoulos, G. Portale, R. W. A. Havenith, S. J. Marrink, J. C. Hummelen, L. J. A. Koster, *Nat. Commun.* **2020**, *11*, 5694; c) H. Sun, X. Guo, A. Facchetti, *Chem* **2020**, *6*, 1310–1326.
[12] a) Y. L. Z. D. Yu, Z. Y. Wang, H. I. Un, S. J. Zelewski, Y. Cui, H.y. You, Y. L. K. F. Xie, Z. F. Yao, Y. C. He, J. Y. Wang, W. B. Hu, H. Sirringhaus, J. Pei, *Sci. Adv.* **2023**, *9*, 3495 ; b) L. I. L. P. F. Odobel, Y. Pellegrin, E. Blart,

Acc. Chem. Res. **2010**, *43*, 1063–1071; c) Z. Wang, P. K. Nayak, J. A. C. Frescas, H. N. Alshareef, *Adv. Mater.* **2016**, *28*, 3831–3892.
[13] a) T. Liu, Y. Yuan, X. Tao, Z. Lin, J. Lu, *Adv. Sci.* **2020**, *7*, 2001207; b) N. Shida, Y. Zhou, S. Inagi, *Acc. Chem. Res.* **2019**, *52*, 2598–2608.
[14] A. E. Lakraychi, F. Dolhem, A. Vlad, M. Becuwe, *Adv. Energy Mater.* **2021**, *11*, 2101562.
[15] a) J. W. Jeon, J. O'Neal, L. Shao, J. L. Lutkenhaus, *ACS Appl. Mater. Interfaces* **2013**, *5*, 10127–10136; b) C. Wang, W. Zheng, Z. Yue, C. O. Too, G. G. Wallace, *Adv. Mater.* **2011**, *23*, 3580–3584; c) T. Zhu, H. Sternlicht, Y. Ha, C. Fang, D. Liu, B. H. Savitzky, X. Zhao, Y. Lu, Y. Fu, C. Ophus, C. Zhu, W. Yang, A. M. Minor, G. Liu, *Nat. Energy* **2023**, *8*, 129–137.
[16] a) F. Meng, M. M. Umair, K. Iqbal, X. Jin, S. Zhang, B. Tang, *ACS Appl. Mater. Interfaces* **2019**, *11*, 13022–13028; b) Z. Song, H. Zhan, Y. Zhou, *Angew. Chem. Int. Ed.* **2010**, *49*, 8444–8448.
[17] a) B. M. P. Cara, N. Gannetta, Luis Melecio-Zambranoa, Colleen Q. Trainora, Brett P. Fors, Héctor D. Abruña, *J. Mater. Chem. A* **2012**, *00*, 1–3; b) Y. Kiya, A. Iwata, T. Sarukawa, J. C. Henderson, H. D. Abruña, *J. Power Sources* **2007**, *173*, 522–530; c) M. López-Herraiz, E. Castillo-Martínez, J. Carretero-González, J. Carrasco, T. Rojo, M. Armand, *Energy Environ. Sci.* **2015**, *8*, 3233–3241.
[18] a) K. Hatakeyama-Sato, H. Wakamatsu, R. Katagiri, K. Oyaizu, H. Nishide, *Adv. Mater.* **2018**, *30*, e1800900; b) T. Janoschka, M. D. Hager, U. S. Schubert, *Adv. Mater.* **2012**, *24*, 6397–6409; c) K. Zhang, Y. Hu, L. Wang, J. Fan, M. J. Monteiro, Z. Jia, *Polym. Chem.* **2017**, *8*, 1815–1823.
[19] a) J. Fanous, M. Wegner, J. Grimminger, M. Rolff, M. B. M. Spera, M. Tenzer, M. R. Buchmeiser, *J. Mater. Chem.* **2012**, *22*, 23240–23245; b) Y. N. Li, Z. Guo, H. Liu, J. Yang, *Electro. Commun.* **2007**, *9*, 1913–1917; c) M. B. Preefer, B. Oschmann, C. J. Hawker, R. Seshadri, F. Wudl, *Angew. Chem. Int. Ed.* **2017**, *56*, 15118–15122.
[20] a) M. Acosta, M. D. Santiago, J. A. Irvin, *Mater.* **2022**, *15*, 8820; b) X. Cao, J. Liu, L. Zhu, L. Xie, *Energy Technol.* **2019**, *7*, 1800759; c) Z. Guo, J. Wang, P. Yu, M. Li, L. Huang, Z. Hu, Y. Wang, Z. Song, *Adv. Energy Mater.* **2023**, *13*, 2301520; d) H. Yang, T. Song, L. Liu, A. Devadoss, F. Xia, H. Han, H. Park, W. Sigmund, K. Kwon, U. Paik, *J. Phys. Chem. C* **2013**, *117*, 17376–17381; e) J. E. Yoo, K. S. Lee, A. Garcia, J. Tarver, E. D. Gomez, K. Baldwin, Y. Sun, H. Meng, T. Q. Nguyen, Y. L. Loo, *PNAS* **2010**, *107*, 5712–5717.
[21] a) Y. Huang, H. Li, Z. Wang, M. Zhu, Z. Pei, Q. Xue, Y. Huang, C. Zhi, *Nano Energy* **2016**, *22*, 422–438; b) M. H. R. Borges, B. E. Nagay, R. C. Costa, J. G. S. Souza, M. T. Mathew, V. A. R. Barão, *Adv. Colloid Interface Sci.* **2023**, *314*, 102860; c) L. Zhou, N. Wang, Y. Chang, S. Zhu, Y. Zhang, W. Hou, Y. Zhao, G. Han, *J. Energy Storage* **2024**, *88*, 111538.
[22] a) T. P. Kaloni, P. K. Giesbrecht, G. Schreckenbach, M. S. Freund, *Chem. Mater.* **2017**, *29*, 10248–10283; b) L. Liu, F. Tian, X. Wang, Z. Yang, M. Zhou, X. Wang, *React. Funct. Polym.* **2012**, *72*, 45–49; c) X. Huang, X. Liu, H. Li, Q. Zhao, T. Ma, *Small Structures* **2022**, *4*, 2200221; d) S. P. Vinodhini, J. R. Xavier, *Mater. Chem. Phys.* **2024**, *318*, 129233.
[23] a) L. W. S. T. R. Jow, M. Maxfield, D. Vernick, *J. Electrochem. Soc.* **1987**, *134*, 1730; b) L. M. Zhu, A. W. Lei, Y. L. Cao, X. P. Ai, H. X. Yang, *Chem. Commun.* **2013**, *49*, 567–569; c) C. Li, W. Wang, Y. Tang, W. Zhuang, J. Zhang, D. Zhang, X. Qian, G. Hong, J. Du, Y. Yao, *Adv. Colloid Interface Sci.* **2025**, *677*, 551–559; d) M. A. A. Mohd Abdah, T. K. Lee, A. Ahmad, Y. Sul·aiman, N. A. Dzulkarnain, M. Mokhtar, M. Khalid, M. S. Su'ait, *ACS Appl. Energ. Mater.* **2023**, *6*, 1605–1620.
[24] J. W. Jeon, Y. Ma, J. F. Mike, L. Shao, P. B. Balbuena, J. L. Lutkenhaus, *Phys. Chem. Chem. Phys.* **2013**, *15*, 9654–9662.
[25] W. Du, X. Du, M. Ma, S. Huang, X. Sun, L. Xiong, *Adv. Funct. Mater.* **2022**, *32*, 2110871.
[26] Z. Song, Y. Qian, T. Zhang, M. Otani, H. Zhou, *Adv. Sci.* **2015**, *2*, 1500124.
[27] G. Dawut, Y. Lu, L. Miao, J. Chen, *Inorg. Chem. Front.* **2018**, *5*, 1391–1396.
[28] H. Dong, Y. Liang, O. Tutusaus, R. Mohtadi, Y. Zhang, F. Hao, Y. Yao, *Joule* **2019**, *3*, 782–793.
[29] D. Du, J. Zhou, Z. Yin, G. Feng, W. Ji, H. Huang, S. Pang, *Adv. Energy Mater.* **2024**, *14*, 2400580.
[30] P. Yu, J. An, Z. Wang, Y. Fu, W. Guo, *Small* **2023**, *20*, 2308881.
[31] J. Y. Zhang, L. B. Kong, L. Z. Zhan, J. Tang, H. Zhan, Y. H. Zhou, C. M. Zhan, *J. Power Sources* **2007**, *168*, 278–281.
[32] L. Xu, F. Yang, C. Su, L. Ji, C. Zhang, *Elect. Acta* **2014**, *130*, 148–155.
[33] C. Han, H. Li, R. Shi, T. Zhang, J. Tong, J. Li, B. Li, *J. Mater. Chem. A* **2019**, *7*, 23378–23415.
[34] X. Chen, X. Yin, J. Aslam, W. Sun, Y. Wang, *Electrochem. Energy Rev.* **2022**, *5*, 12.
[35] H. Peng, J. Xiao, Z. Wu, L. Zhang, Y. Geng, W. Xin, J. Li, Z. Yan, K. Zhang, Z. Zhu, *CCS Chem.* **2023**, *5*, 1789–1801.
[36] R. Shi, L. Liu, Y. Lu, C. Wang, Y. Li, L. Li, Z. Yan, J. Chen, *Nat. Commun.* **2020**, *11*, 178.
[37] Y. Lu, Q. Zhang, L. Li, Z. Niu, J. Chen, *Chem* **2018**, *4*, 2786–2813.
[38] Z. Li, Y.. Zhang, J. Xu, Y. G. Wang, *Batteries & Supercaps* **2023**, *6*, e202200431.
[39] X. Liu, X. Wang, Z. Ye, *Adv. Funct. Mater.* **2023**, *33*, 2302618.
[40] H. Kim, J. E. Kwon, B. Lee, J. Hong, M. Lee, S. Y. Park, K. Kang, *Chem. Mater.* **2015**, *27*, 7258–7264.
[41] S. Lee, J. E. Kwon, J. Hong, S. Y. Park, K. Kang, *J. Mater. Chem. A* **2019**, *7*, 11438–11443.
[42] M. Tang, S. Zhu, Z. Liu, C. Jiang, Y. Wu, H. Li, B. Wang, E. Wang, J. Ma, C. Wang, *Chem.* **2018**, *4*, 2600–2614.
[43] M. Tang, Y. Wu, Y. Chen, C. Jiang, S. Zhu, S. Zhuo, C. Wang, *J. Mater. Chem. A* **2019**, *7*, 486–492.
[44] C. Q. Li, A. Yu, W. K. Zhao, G. K. Long, Q. C. Zhang, S. L. Mei, C. J. Yao, *Angew. Chem. Int. Ed.* **2024**, *63*, e202409421.
[45] K. Fan, J. Li, Y. Xu, C. Fu, Y. Chen, C. Zhang, G. Zhang, J. Ma, T. Zhai, C. Wang, *J. Am. Chem. Soc.* **2023**, *145*, 12682–12690.
[46] C. N. Gannett, L. Melecio-Zambrano, M. J. Theibault, B. M. Peterson, B. P. Fors, H. D. Abruña, *J. Mater.* **2021**, *1*, 100008.
[47] H. Peng, J. Xiao, Z. Wu, L. Zhang, Y. Geng, W. Xin, J. Li, Z. Yan, K. Zhang, Z. Zhu, *CCS Chem.* **2023**, *5*, 1789–1801.
[48] A. Vlad, J. Rolland, G. Hauffman, B. Ernould, J. F. Gohy, *CSSC.* **2015**, *8*, 1692–1696.
[49] F. Xing, S. Li, L. Chen, J.-S. Dang, X. He, *ACS Nano* **2023**, *17*, 21432–21442.
[50] S. Wang, Q. Wang, P. Shao, Y. Han, X. Gao, L. Ma, S. Yuan, X. Ma, J. Zhou, X. Feng, B. Wang, *J. Am. Chem. Soc.* **2017**, *139*, 4258–4261.
[51] C. Wang, Q. Ji, R. Chu, Z. Ullah, M. Zheng, X. Dong, Y. Sun, Q. Li, L. Liu, *ACS Appl. Energ. Mater.* **2021**, *4*, 12641–12648.
[52] R. Shi, L. Liu, Y. Lu, Y. Li, S. Zheng, Z. Yan, K. Zhang, J. Chen, *Adv. Energy Mater.* **2020**, *11*, 2002917.
[53] G. Wang, N. Chandrasekhar, B. P. Biswal, D. Becker, S. Paasch, E. Brunner, M. Addicoat, M. Yu, R. Berger, X. Feng, *Adv. Mater.* **2019**, *31*, 1901478.
[54] Y. L. Wang, Y. H. Zhu, Z. X. Chen, X. Yang, R. Y. Zhang, H. G. Wang, Y. K. Yang, *Angew. Chem. Int. Ed.* **2024**, *136*, e202401253.
[55] Z. Luo, L. Liu, J. Ning, K. Lei, Y. Lu, F. Li, J. Chen, *Angew. Chem. Int. Ed.* **2018**, *57*, 9443–9446.
[56] Z. Xiao, G. Xiang, Q. Zhang, Y. Wang, Y. Yang, *Energy Environ. Mater.* **2022**, *6*, e12399.
[57] G. Zhou, Y. E. Miao, Z. Wei, L. Mo, F. Lai, Y. Wu, J. Ma, T. Liu, *Adv. Funct. Mater.* **2018**, *28*, 1804629.

Manuscript received: September 14, 2024
Revised manuscript received: October 27, 2024
Accepted manuscript online: November 12, 2024
Version of record online: November 25, 2024